

Solving relativistic hydrodynamic equation in presence of magnetic field for phase transition in a neutron star

Ritam Mallick¹, Rajesh Gopal², Sanjay k Ghosh², Sibaji Raha²
& Suparna Roychowdhury³

¹ Institute of Physics, Bhubaneswar 751005, Orissa, INDIA

² Centre for Astroparticle Physics and Space Science; Bose Institute; Block - EN, Sector V; Salt Lake; Kolkata - 700091; INDIA

³ Department of Physics; St. Xaviers College; Kolkata - 700016; INDIA

E-mail: ritam.mallick5@gmail.com

Abstract. Hadronic to quark matter phase transition may occur inside neutron stars (NS) having central densities of the order of 3-10 times normal nuclear matter saturation density (n_0). The transition is expected to be a two-step process; transition from hadronic to 2-flavour matter and two-flavour to β equilibrated charge neutral three-flavour matter. In this paper we concentrate on the first step process and solve the relativistic hydrodynamic equations for the conversion front in presence of high magnetic field. Lorentz force due to magnetic field is included in the energy momentum tensor by averaging over the polar angles. We find that for an initial dipole configuration of the magnetic field with a sufficiently high value at the surface, velocity of the front increases considerably.

PACS numbers: 26.60.Kp, 97.10.Cv

1. Introduction

Study of strongly interacting matter at high density and/or temperature is of immense current interest. As proposed in [1, 2] a form of matter consisting of almost equal numbers of up (u), down (d) and strange (s) quarks, may be the true ground state of strongly interacting matter at high densities and/or temperature. This conjecture is supported by Bag model calculations [3] for certain range of values of the strange quark mass and the strong coupling constant. This form of bulk matter consisting of u, d, and s quarks is referred to as "strange quark matter (SQM)".

The extreme conditions of high density and/or temperature can be envisaged through at least two scenarios; one being the terrestrial lab in which such conditions can be reproduced (like controlled study of elementary particle interactions at high energies) and the other being the astrophysical lab of compact objects. Some advancement has already been made to recreate the deconfinement transition in the collision of heavy nuclei in high energy accelerators *e.g.* at CERN-SPS in Geneva and RHIC in Brookhaven national laboratory (BNL). Along with the above terrestrial laboratories, compact stars having central density as high as 3-10 times nuclear matter saturation density, can be used to test nature of strongly interacting matter.

High density inside NSs is expected to induce a transition to quark matter. If SQM is the true ground state of strongly interacting matter, as conjectured by Witten [1], then there is a novel possibility that some NSs can get completely converted to SS. Some tentative SS candidates are the compact objects associated with X-ray bursters GRO J1744 – 28 [4], SAX J1808.4 – 3658 [5] and X-ray pulsars Her X – 1 [6].

A mechanism of the phase transition from NS to SS was first proposed by Alcock et al. [7]. They argued that the conversion process starts when the star comes in contact with an external strange quark nugget seed. Glendenning ([8]) on the other hand suggested that the conversion may begin when there is a sudden spin down of a neutron star. The abrupt change in the angular velocity of the star suddenly increases the central (or core) density thereby triggering the phase transition process.

Several authors has studied the hadronic to quark matter conversion. Olinto [9] considered the phase transition of hadronic to SQM as a weak interaction process and evaluated the front velocity assuming it to be a slow-combustion. Olesen and Madsen [10] and Heiselberg et al. [11] found the speed of conversion to be in the range between 10 m/s to 100 km/s. Conversion of hadronic to two-flavour quark matter in the astrophysical scenario was studied by Collins and Perry [12]. They argued that the hadronic matter, at first, undergoes deconfinement to quark matter and then eventually decays to three-flavour matter through weak process. A non-relativistic hydrodynamic stability analysis of such combustion process was done by Horvath and Benvenuto [13]. Cho et al. [14] improved it further and used a relativistic framework to examine the conservation condition of energy-momentum and baryonic density flux across the conversion front. Tokareva et al. [15] studied the conversion process assuming it to be detonation shock front. On the other hand, Berezhiani et al. [16], Bombaci et al. [17]

and Drago et al. [18], related it with gamma ray bursts, suggesting that the formation of SQM may be delayed if the deconfinement process takes place through a first order transition [19]. The two-step process was again recently considered by Bombaci et al. and other authors [20, 21]. More recent development on the subject includes the dynamical simulations of the combustion process both in 1D ([22]) and in 3D ([23]).

Most of the works however have not incorporated some of the important features of NS, namely the rotational and the general relativistic (GR) effects. We have tried to incorporate these effects systematically in a series of works. We have shown [24] that the conversion process is most likely a two-step process. Following Glendenning we heuristically assumed the existence of conversion front originating at the center and propagating outwards. The first step involved the conversion of NS to a two-flavour QS. We assumed the central density to be high, $(3 - 10)$ times normal matter density, and that the transition front proceeds as a detonation. We found that within a few milliseconds the NS gets converted to a metastable two-flavour QS. The second step corresponds to the conversion of two-flavour quark matter to the stable three-flavour SQM, through weak interaction. We have also exhibited [25] the major role played by the GR effects in the rotating stars; the conversion fronts, corresponding to the nuclear to two-flavour matter conversion, propagate with different radial velocities in different directions.

Identifying pulsars with rotating NS leads to the conclusion that NS have very high magnetic fields ($10^{10} - 10^{12}$ G) at the surface. The origin of such magnetic fields in NS remains unclear till date; even if all magnetic lines of force were to be trapped during the collapse, one would estimate [26] a surface field of $10^8 - 10^9$ G. The observed slow-down rate of pulsars require surface magnetic fields in the range of $10^{10} - 10^{12}$ G. The canonical picture of the classical pulsar mechanism involves [26] a magnetic dipole at the center of a rotating NS. In one of our ongoing project [27] we have tried to include the effect of magnetic field in the general relativistic framework through the introduction of a Lorentz force on the equation of motion by hand. As opposed to the present case where only dipolar configuration has been assumed, in [27] we have studied other different magnetic field configuration as well. For the dipolar field the nature of front propagation remains more or less same (only slight change in velocity). One of the interesting findings of [27] is that if the magnetic field is of planar radial nature which decreases towards the surface, the term due to the magnetic field opposes the front velocity. If the magnetic field is quite high then it may stall the front inside the star and much higher values of magnetic field stops the front from taking off.

In the present work our effort is to incorporate the effect of the magnetic field on the equation of motion starting from the conservation equation. Moreover, we try to have an understanding of the angular dependence of the magnetic field by averaging the Lorentz force over the polar angles. Since this is our first attempt, we have limited our study to the special relativistic case and present the findings after the incorporation of the magnetic field in the relativistic hydrodynamic equations for the conversion of nuclear matter to two-flavour quark matter. We have performed our calculation with

zero viscosity and resistivity, that is in the ideal hydrodynamic approximation.

To study the conversion process, we have considered the relativistic EOSs describing the forms of the matter in respective phases. Due to the propagation of the shock wave, the properties of the medium on either side of the shock exhibit a discontinuity. We have studied the various conservation conditions on either side of the front. Development of the conversion front, as it propagates radially through the model star in the presence of magnetic field, has been examined. Here, we have considered very slowly rotating neutron star so that we can use the static limits. In section II, we discuss the EOSs and the initial jump conditions. In section III, we present the governing equations for the combustion front propagation by incorporating the effect of the Lorentz force due to the magnetic field. In section IV, we present the results obtained by solving the relativistic MHD equations. Conclusions that may be drawn from these results are presented in the final section.

2. Initial jump condition

The nuclear matter phase is described by the non-linear Walecka model [28] and the quark phase by the MIT Bag model [7], quark numbers being fixed by the number of baryons in the nuclear phase. We treat both the nuclear and quark phases as ideal fluids.

The nuclear matter EOS has been evaluated using the nonlinear Walecka model [28]. The Lagrangian density in this model is given by:

$$\begin{aligned} \mathcal{L}(x) = & \sum_i \bar{\psi}_i (i\gamma^\mu \partial_\mu - m_i + g_{\sigma i} \sigma + g_{\omega i} \omega_\mu \gamma^\mu - g_{\rho i} \rho_\mu^a \gamma^\mu T_a) \psi_i - \frac{1}{4} \omega^{\mu\nu} \omega_{\mu\nu} \\ & + \frac{1}{2} m_\omega^2 \omega_\mu \omega^\mu + \frac{1}{2} (\partial_\mu \sigma \partial^\mu \sigma - m_\sigma^2 \sigma^2) - \frac{1}{4} \rho_{\mu\nu}^a \rho_a^{\mu\nu} + \frac{1}{2} m_\rho^2 \rho_\mu^a \rho_a^\mu \\ & - \frac{1}{3} b m_n (g_{\sigma N} \sigma)^3 - \frac{1}{4} C (g_{\sigma N} \sigma)^4 + \bar{\psi}_e (i\gamma^\mu \partial_\mu - m_e) \psi_e \end{aligned} \quad (1)$$

The Lagrangian in equation (1) includes nucleons (neutrons and protons), electrons, isoscalar scalar, isoscalar vector and isovector vector mesons denoted by ψ_i , ψ_e , σ , ω^μ and $\rho^{a,\mu}$, respectively. The Lagrangian also includes cubic and quartic self interaction terms of the σ field. The parameters of the nonlinear Walecka model are meson-baryon coupling constants, meson masses and the coefficient of the cubic and quartic self interaction of the σ mesons (b and c, respectively). The meson fields interact with the baryons through linear coupling. The ω and ρ meson masses have been chosen to be their physical masses. The rest of the parameters, namely, nucleon-meson coupling constant ($\frac{g_\sigma}{m_\sigma}$, $\frac{g_\omega}{m_\omega}$ and $\frac{g_\rho}{m_\rho}$) and the coefficient of cubic and quartic terms of the σ meson self interaction (b and c, respectively) are determined by fitting the nuclear matter saturation properties, namely, the binding energy/nucleon (-16 MeV), baryon density ($\rho_0=0.17 \text{ fm}^{-3}$), symmetry energy coefficient (32.5 MeV), Landau mass ($0.83 m_n$) and nuclear matter incompressibility (300 MeV).

In the present paper, we first consider the conversion of nuclear matter, consisting of only nucleons (*i.e.* without hyperons) to a two-flavour quark matter. The final composition of the quark matter is determined from the nuclear matter EOS by enforcing the baryon number conservation during the conversion process. That is, for every neutron two down and one up quarks and for every proton two up and one down quarks are produced, electron number being same in the two phases. The mass of the up and down quarks are taken to be 5 MeV and 10 MeV respectively. The value of the bag constant is taken to 160 MeV. The pressure-density relation of the two models are depicted in fig. 1.

Recently, after the discovery of high-mass pulsar PSR J1614-2230 [29] the EOSs describing the interior of a compact star have been put to severe constraint. Mostly EOS with 'exotic' matter such as hyperons and kaon condensates which cannot generate high-mass stars within a range of central densities are now under speculations. In [29] typical values of the central density of J1614-2230, for the allowed EOSs is in the range $2n_0$ - $5n_0$. On the other hand, consideration of the EOS independent analysis of [30] sets the upper limit of central density at $10n_0$.

We have shown the mass-radius curve in fig. 2 for both hadronic and metastable two-flavour quark matter EOS. In Table 1 we have given the number density, mass and radius of stars made of hadronic matter, two-flavour metastable as well as three-flavour, β equilibrated charge neutral matter. It is found that though both the hadronic as well as two-flavour matter with bag pressure of 160 MeV are within the range of parameters as suggested by Demorest et al., three-flavour matter with the same bag pressure has smaller mass. A lower bag pressure of 145 MeV is needed to nearly reach the limits of [29]. Here we should mention that similar calculation done by other authors agrees with our results given in the Table 1. Recent calculation by Zudnik et al., Bauswein et al. and Weissenborn et al. [31, 32, 33] found that the maximum masses of the strange star is just below 2 solar masses with bag pressure 145 MeV. There they have used MIT bag model to construct the star with strange quark mass of 100 MeV. In Table 1 we have shown strange star masses of bag pressure 145 MeV and 160 MeV. We have shown results for strange quark masses of 50 MeV, 100 MeV, 150 MeV and 200 MeV, and our results are at par with the other previous calculations. As the mass of strange quark mass is still debated, for a range of strange quark mass we find that the maximum mass of the strange star with bag pressure 160 MeV is 1.6 times mass of sun (M_\odot), which is smaller than that prescribed by Demorest et al.. The limitation of bag model itself, as has been shown in [34], is another important issue. Under the present circumstances, one may have to consider other options such as a strongly interacting system, a more involved picture as given in [34] or other effective models such as PNJL [35] to repeat the similar calculations. However, in the present work we have concentrated on the effect of magnetic field on the front using the simple bag model picture and the EOS here is needed for estimating the initial velocity of the front. The effect of bag pressure and hence equation of state is of course important as the physical values of velocity is obtained only within a narrow range of ± 5 MeV around 160 MeV bag pressure [24]. We

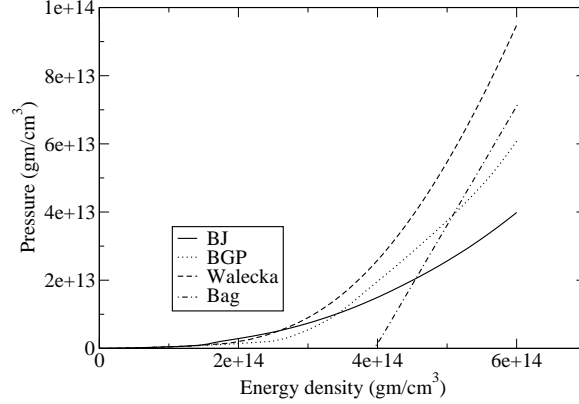


Figure 1. Pressure vs. energy density plot for different model EOS.

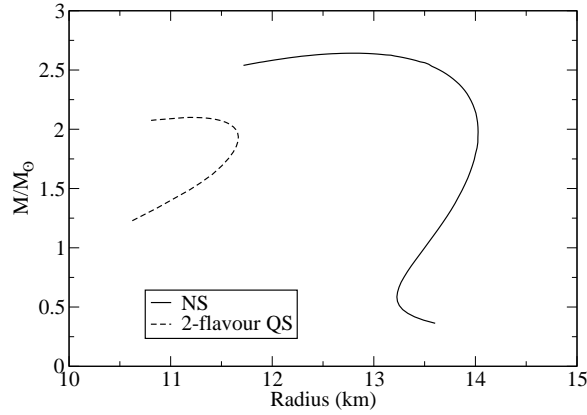


Figure 2. Mass-radius plot for NS and two-flavour quark star, with bag constant 160 MeV.

have repeated our calculation for various densities and discussed the results for $4n_0$ for illustration.

Following the picture of Glendenning [8] we have assumed that the phase transition is initiated by a sudden spin down of the star. So let us now consider the physical situation where a combustion front has been generated in the core of the neutron star. This front propagates outwards through the neutron star with a certain hydrodynamic velocity, leaving behind a u-d-e matter. We denote all the physical quantities in the hadronic sector by subscript 1 and those in the quark sector by subscript 2.

Quantities on opposite sides of the front are related through the energy density, the momentum density and the baryon number density flux conservation [15, 36, 37]. In the rest frame of the combustion front, the velocities of the matter in the two phases, are written as [36]:

$$v_1^2 = \frac{(p_2 - p_1)(\epsilon_2 + p_1)}{(\epsilon_2 - \epsilon_1)(\epsilon_1 + p_2)}, \quad (2)$$

Table			
EOS	n_B/n_0	M/M_\odot	R in km
Walecka	4	1.9	14
	6	2.45	13.7
	8	2.58	13.4
Bag 160 MeV 2-flav.	4	1.63	11.3
	6	1.99	11.7
	8	2.1	11.6
Bag 145 MeV 2-flav.	4	2.07	12.2
	6	2.26	12.0
	8	2.32	11.8
Bag 160 MeV 3-flav. $m_s=50$ MeV	4	1.05	9.74
	6	1.46	9.95
	8	1.59	9.74
Bag 160 MeV 3-flav. $m_s=100$ MeV	4	0.92	9.15
	6	1.37	9.51
	8	1.51	9.4
Bag 160 MeV 3-flav. $m_s=150$ MeV	4	0.88	9.32
	6	1.19	9.59
	8	1.32	9.60
Bag 160 MeV 3-flav. $m_s=200$ MeV	4	0.79	9.03
	6	1.11	9.34
	8	1.23	9.36
Bag 145 MeV 3-flav. $m_s=50$ MeV	4	1.75	11.9
	6	1.93	11.7
	8	1.97	11.5
Bag 145 MeV 3-flav. $m_s=100$ MeV	4	1.67	11.7
	6	1.87	11.4
	8	1.92	11.1
Bag 145 MeV 3-flav. $m_s=150$ MeV	4	1.64	11.5
	6	1.8	11.4
	8	1.86	11.4
Bag 145 MeV 3-flav. $m_s=200$ MeV	4	1.54	11.3
	6	1.76	11.2
	8	1.81	11.1

Table 1. Tabulated ratio of number density, mass and radius for stars with different EOS

and

$$v_2^2 = \frac{(p_2 - p_1)(\epsilon_1 + p_2)}{(\epsilon_2 - \epsilon_1)(\epsilon_2 + p_1)}. \quad (3)$$

3. Propagation of combustion front in the presence of Magnetic field

The preceding discussion is mainly a feasibility study for the possible generation of the combustive phase transition front. Using it to be the initial condition, we now study the evolution of the hydrodynamical combustion front in the presence of magnetic field. Following our recent work [24], we choose a regime where the propagation front moves as a detonation front. To examine such an evolution, we move to a reference frame in which the nuclear matter is at rest. The speed of the combustion front in such a frame is given by $v_f = -v_1$ with v_1 being the velocity of the nuclear matter in the rest frame of the front.

In this section we study the time evolution of the shock front within the special relativistic formalism in the presence of the static background magnetic field in the neutron star. The energy momentum tensor of an ideal fluid in the presence of a magnetic field can be written as the sum of the matter energy momentum tensor $T_{\mu\nu}^M$ and the magnetic energy momentum tensor $T_{\mu\nu}^B$. The matter energy momentum tensor can be written as:

$$T_{\mu\nu}^M = (p + \epsilon) u_\mu u_\nu + p \eta_{\mu\nu}$$

where, the fluid four velocity is $u_\mu = \Gamma(1, \vec{v})$, Γ is the Lorentz factor and \vec{v} is the fluid three velocity. The pressure and energy density p and ϵ are evaluated in the rest frame of the fluid.

The magnetic energy momentum tensor can be written in terms of its components as:

$$\begin{aligned} T_{00} &= \frac{B^2}{8\pi} \\ T_{0i} &= 0 \\ T_{ij} &= \frac{B^2}{8\pi} \delta_{ij} - \frac{B_i B_j}{4\pi} \end{aligned}$$

In writing down the components of the magnetic tensor, we have assumed that the electric field is zero in the nuclear matter rest frame. Hence T_{0i} which is simply the Poynting flux vector is zero. The equations of motion follow from the covariant conservation of the total energy momentum tensor $\partial_\nu T^{\mu\nu} = 0$. Thus we can write, $\partial_\nu T_{\mu\nu}^M = -\partial_\nu T_{\mu\nu}^B$. The expression on the right hand side in the above expression is simply the Lorentz four force f^μ . The zeroth component of the four force f^0 is zero since there is no electric fields whereas the three-force is the Lorentz force due to magnetic field $\vec{F} = (\nabla \times \vec{B}) \times \vec{B}$.

Using the above arguments we can write down the hydrodynamic equation for the propagation of the transition front [24] in the presence of the magnetic field:

$$\frac{1}{\omega} \left(\frac{\partial \epsilon}{\partial \tau} + v \frac{\partial \epsilon}{\partial r} \right) + \frac{1}{W^2} \left(\frac{\partial v}{\partial \tau} + v \frac{\partial v}{\partial r} \right) + 2 \frac{v}{r} = 0 \quad (4)$$

and

$$\frac{1}{\omega} \left(\frac{\partial p}{\partial \tau} + v \frac{\partial p}{\partial r} \right) + \frac{1}{W^2} \left(\frac{\partial v}{\partial \tau} + v \frac{\partial v}{\partial r} \right) = \frac{\langle F_r \rangle}{4\pi\omega}, \quad (5)$$

where, $v = \frac{\partial r}{\partial \tau}$ is the front velocity in the nuclear matter rest frame and $k = \frac{\partial p}{\partial \epsilon}$ is taken as the square of the effective sound speed in the medium. p , ϵ , ω and W are the pressure, energy density, enthalpy and Lorentz factor respectively.

The effect of magnetic fields is included through the Lorentz force as given in eqn. 5. The energy equation is unaffected since we assume that the conductivity is formally infinite so that there are no dissipative effects. It is also to be noted that we have included the Lorentz force by considering its average over the polar angles. The Lorentz force term is not spherically symmetric. As a result, the shock speed would also vary with direction. As we are concerned only with the radial propagation (spherically symmetric star), we have considered approximate angle averages to incorporate the effect of angle dependence. The details of the different configurations and the corresponding forms for the Lorentz force are detailed in the Appendix.

Equations (4) and (5) can be rewritten as:

$$\frac{2v}{\omega} \frac{\partial \epsilon}{\partial r} + \frac{1}{W^2} \frac{\partial v}{\partial r} (1 + v^2) + \frac{2v}{r} = 0 \quad (6)$$

and

$$\frac{n}{\omega} \frac{\partial \epsilon}{\partial r} (1 + v^2) + \frac{2v}{W^2} \frac{\partial v}{\partial r} = \frac{\langle F_r \rangle}{4\pi\omega} \quad (7)$$

We finally get a single differential equation for the front velocity:

$$\frac{dv}{dr} = \frac{1}{W^2[4v^2 - k(1 + v^2)^2]} \left[\frac{\langle F_r \rangle}{4\pi\omega} + \frac{k(1 + v^2)}{r} \right] \quad (8)$$

The above equation is integrated with respect to r from the center to the surface. The initial velocity is fixed through the jump conditions for different values of the central densities. The magnetic field is incorporated by specifying different configurations.

4. Results

Equations (2) and (3) specify the respective flow velocities v_1 and v_2 of the nuclear and quark matter in the rest frame of the front. This would give us the initial velocity of the front ($-v_1$), at a radius infinitesimally close to the center of the star, in the nuclear matter rest frame. The nuclear matter EOS (Walecka model) has been used to construct the static configuration of compact star, for different central densities, by using the standard Tolman-Oppenheimer-Volkoff (TOV) equations [38, 39]. The velocity at the center of the star should be zero from symmetry considerations. On the other hand, the $1/r$ dependence of the $\frac{dv}{dr}$, in eq. (8) suggests a steep rise in velocity near the center of the star. Equation (8) is then integrated, with respect to r , starting from the center towards the surface of the star. The solution gives us the variation of the velocity with the position as a function of time of arrival of the front, along the radius of the star.

In this section, we present the results of the velocity profiles for different magnetic field strength for dipole configurations. We first consider a poloidal magnetic field which

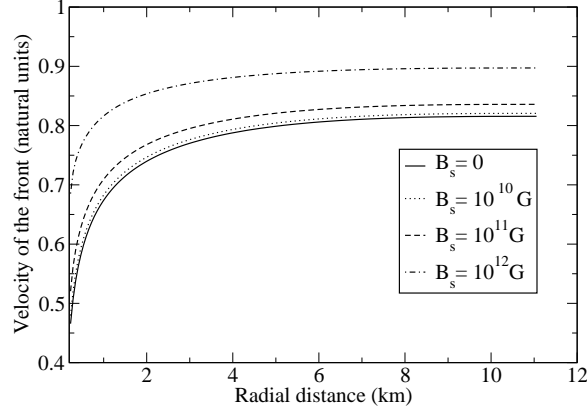


Figure 3. Variation of velocity of the conversion front along the radial distance of the star for various values of the surface magnetic field.

can be specified in terms of the field components as:

$$\begin{aligned} B_r &= \frac{B_0 \sin \theta}{r^3} \\ B_\theta &= \frac{2B_0 \cos \theta}{r^3} \end{aligned} \quad (9)$$

In the magnetic field profile, r is the distance from the center while B_0 is related to the surface magnetic field B_S through $B_0 = B_S R^3$, where R is the radius of the star. As the interior of the star is hidden from direct observation we only know about the surface magnetic field of the star. Therefore, in this work we would always quote the surface magnetic field value. In our calculation the front starts from a distance of 100 – 200m from the center of the star. Therefore surface field of 10^{10}G and 10^{12}G would have a value of 10^{16}G and 10^{18}G respectively at the starting point of our calculation. These values are within the maximum allowed field value for the stability of magnetized neutron stars [40]. The angle averaged Lorentz force $\langle F_r \rangle$ for this configuration is $\langle F_r \rangle = \frac{B_0^2}{12\pi r^7}$ as evaluated in the appendix.

In fig. 3, we show the propagation velocity of the conversion front along the radius of the star with a central density of 4 times nuclear matter saturation density. The solid curve denotes the SR calculation without the consideration of the magnetic field. The dotted curve is for SR calculation with a surface magnetic field of dipolar nature of strength 10^{10} Gauss. Below this field the effect of magnetic field on the conversion front is very negligible. The curve shows that the magnetic field enhances the velocity of the front which is also clear from equation (8). Next we increase the magnetic field strength and the subsequent curves on the figure shows that the velocity of the conversion front increases with the increase of field strength. We also find that the magnetic field effect is much pronounced at the center of the star. This is because as we go towards the center the magnetic field increases as r^3 , as given in eqn 9. So although the density increases the magnetic field increases much rapidly towards the center of the star.

Fig. 4 shows the velocity of the conversion front along the radial direction of the

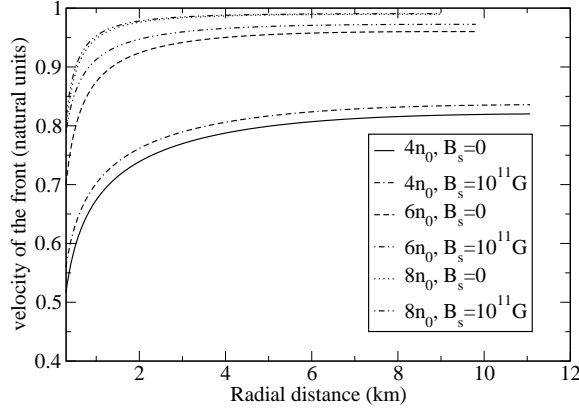


Figure 4. Variation of velocity of the conversion front along the radial direction with a surface magnetic field of strength of 10^{11} Gauss for different values of the central density.

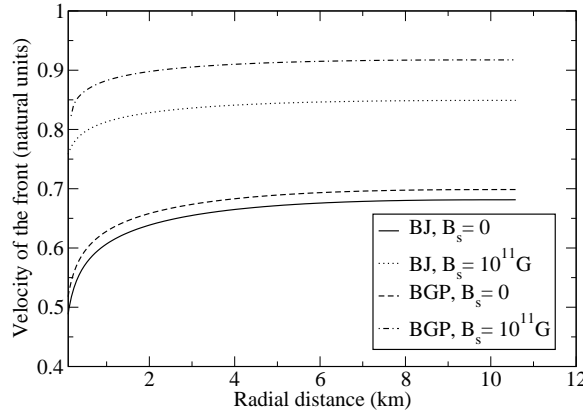


Figure 5. Variation of velocity of the conversion front along the radial direction with a surface magnetic field of strength 10^{11} Gauss for two different EOS namely BGP and BJ.

star for different central densities of the star. The solid curve is for the central density 4 times that of nuclear matter saturation density (n_0) without magnetic field effect. The dash-dash-dot curve is for the same central density with a surface magnetic field of 10^{11} Gauss. As expected we find that velocity of the front increases with the magnetic field. Next we increase the central density, and the two other set of curves are for the central densities corresponding to 6 times and 8 times that of nuclear matter saturation density respectively. The comparison with and without magnetic field is done with same value of the surface magnetic field (10^{11} Gauss). We find that as the central density increases the velocity of the propagating front also increases. This is due to the fact that the velocity of the front depends on the value of k (equation (8)), or the stiffness of the EOS. For a high central density the star is more compact and therefore k is much larger resulting in the further increase of the velocity. We also find that for the same value

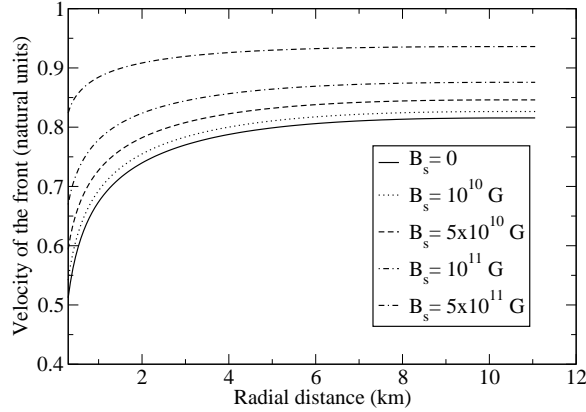


Figure 6. Variation of velocity of the conversion front along the radial direction for different magnetic field strength for toroidal field.

of magnetic field as the density increases the effect of magnetic field decreases. This is because the denser the matter greater the magnetic field has to be applied to have the same effect as the matter pressure is higher at higher densities. So the magnetic pressure has to be higher to be in comparison with the matter pressure to be able to show significant change.

Similar calculation with central density 4 times that of nuclear saturation density is done for two other different EOS, Bowers, Gleeson and Pedigo (BGP) model [41] and Bethe and Johnson (BJ) model [42]. Fig. 5 shows the velocity of the front for these two models with and without the effect of magnetic field. The surface magnetic field applied for the two cases is same (10^{11} Gauss). We again find that the magnetic field increases the velocity of the propagation front. As the BGP model being much stiffer than the BJ model EOS, the velocity of the front is larger for the BGP model compared to that of the BJ model. Therefore we find that the velocity of the front depends on the central density as well as the EOS we choose. The velocity increases with the increase in magnetic field. Below a certain value of the field the effect on the conversion front is not at all relevant and for a very high value of magnetic field (which may be found in magnetars) the velocity of the front attains a velocity close to that of the speed of light.

Little is known about the magnetic field structure in neutron star, and therefore it is not good enough to assume that only poloidal field would be present. In fact, a proto-neutron star dynamo [43] is unlikely to generate purely poloidal field and differential rotation will easily wrap any poloidal field and generate strong toroidal field [44]. Therefore it seems realistic to consider effect of magnetic field configuration consisting of poloidal and toroidal components. The toroidal magnetic field grows from the poloidal dipole field. This can be possible for the differential rotation (ω_d) usually present in the neutron stars [45, 46]. The velocity due to the differential rotation can be written as

$$V_d = \omega_d r \hat{\phi}. \quad (10)$$

As nothing specific is known about the differential rotation, for simplification, we assume

ω_d to be constant and equal to 1. So that it can be taken care of along with the normalization constant. The toroidal field B_T due to this differential rotation is given by

$$B_T = \nabla \times (V_d \times B) \quad (11)$$

where B is the dipole field. Hence we get,

$$B_T = -\frac{B_0 \sin \theta}{r^3} \hat{\phi} \quad (12)$$

with some constant which we have normalized. Using the equation given in the appendix for the toroidal field, the angle averaged Lorentz force $\langle F_r \rangle$ for this configuration is found to be $\langle F_r \rangle = \frac{B_0^2}{2\pi r}$. In fig. 6 we have plotted the velocity of the conversion front for the toroidal field. As we have averaged out the Lorentz force over the polar angle the angle averaged Toroidal field comes out to be of the same form as the poloidal force (see appendix). The nature of the curve remains same, as the angle averaged toroidal field is just six times than that of the poloidal field. Therefore a much lesser value of surface magnetic field is needed to generate the same effect in the conversion front velocity than that needed for the poloidal field. However the main factor for the toroidal field configuration remains the time and the value of the differential rotation of the star.

5. Summary and Discussion

To summarize, we have studied the effect of magnetic field in the phase transition of NS to two-flavour QS. We have incorporated a Lorentz force in the equation of motion for the propagation of a front across the star converting the NS to two-flavour QS. We have assumed a field of dipolar nature with a field strength of maximum 10^{18}G near the center of the star from where our calculation begins.

We find that the velocity of the front increases with the increase of magnetic field strength. We have also calculated the velocity of the front for different central density with same magnetic field of 10^{11}G at the surface. We find that the velocity of the front increases with the increase in central core density of the star. We have done an analytical calculation for different types of field configuration (in the appendix) and for an initial field of dipolar nature, and have shown our results for poloidal and toroidal configuration. For a field of dipolar nature there is an increment of about 10 percent in the front velocity for a field strength of 10^{18}G near the center. In our calculation of angular averaging we find that the toroidal angle average field is 6 times more stronger than the poloidal angle average value. Therefore the effect of magnetic field for toroidal case is much more pronounced.

It should be mentioned at this point that an earlier set of authors [47] studied the effect of an idealized configuration of the magnetic field - a constant magnetic field of moderate strength of $\sim 10^{12-13}\text{G}$ in a dipolar geometry - on the Rayleigh-Taylor (RT) instability. Through an order of magnitude estimate, they concluded that there would be a difference in the velocity of the combustion front along polar and equatorial

directions. Our calculation is based on initial dipolar magnetic field with a high value of magnetic field at the center. Our previous work with magnetic field was interesting but the origin of magnetic force on the equation of motion was truly put by hand. As this is a first attempt of such kind, to have an overall understanding of the magnetic effect on propagation front, starting from the tensorial conservation equation, we have done averaging in the angular direction. For small value of magnetic field it is quite acceptable, but for high value of magnetic field effect of angular dependence may become more pronounced. The present study gives a good estimation of the effect of magnetic field on the propagation speed through an order of magnitude estimation. To get finer details, we need to solve general MHD equation in presence of all the components. As the exact nature of the field configuration is not known, we need to carry out similar calculation with other forms of magnetic field. Furthermore, such high magnetic fields can even modify the Einstein equation for the metric as the matter is then no longer an ideal fluid. All such a calculation is on our immediate agenda.

5.1. Appendix : Angle -averaged radial Lorentz force

The Lorentz force due to a magnetic field B is given by

$$\vec{F} = \frac{(\nabla \times \vec{B}) \times \vec{B}}{4\pi} \quad (13)$$

This can also be written as :

$$4\pi\vec{F} = -\frac{1}{2}\nabla(B^2) + (\vec{B} \cdot \nabla)\vec{B} \quad (14)$$

Using spherical coordinates, the radial component of the Lorentz force can be simplified as [48],

$$4\pi F_r = \nabla \cdot (B_r \vec{B}) - \frac{B_T^2}{r} - \frac{1}{2} \frac{\partial}{\partial r} (B^2) \quad (15)$$

Here, $B_T^2 = B_\phi^2 + B_\theta^2$, denotes the transverse part of the expression. The angle averaged Lorentz force is defined as:

$$\langle F_r \rangle = \int \frac{d\Omega}{4\pi} F_r \quad (16)$$

Taking the angular average of Eq (15), we get:

$$4\pi \langle F_r \rangle = \langle \nabla \cdot (B_r \vec{B}) \rangle - \frac{\langle B_T^2 \rangle}{r} - \frac{1}{2} \frac{\partial}{\partial r} (\langle B^2 \rangle) \quad (17)$$

The angle average of $\langle \nabla \cdot (\vec{B} B_r) \rangle$ can be easily evaluated. Let

$$f(r) = \langle \nabla \cdot (\vec{B} B_r) \rangle = \int \frac{d\Omega}{4\pi} \nabla \cdot (\vec{B} B_r) \quad (18)$$

Multiplying both sides by $r^2 dr$ and integrating,

$$\int dr r^2 f(r) = \int \frac{dV}{4\pi} \nabla \cdot (\vec{B} B_r). \quad (19)$$

Using Stokes theorem, the right hand side of the volume integral can be expressed as a surface integral,

$$\int dr r^2 f(r) = r^2 \int \frac{d\Omega}{4\pi} \hat{r} \cdot (\vec{B} B_r) \quad (20)$$

Now, differentiating both sides w.r.t r we get:

$$f(r) = \frac{1}{r^2} \frac{d}{dr} (r^2 \langle B_r^2 \rangle) \quad (21)$$

Using Eq (16), Eq (18) and the fact that $B^2 = B_r^2 + B_\theta^2 + B_\phi^2$, the final expression for the angle-averaged radial force can be written in terms of the angle average of the different components as:

$$4\pi \langle F_r \rangle = \frac{1}{2} \frac{d}{dr} [\langle B^2 \rangle - 2\langle B_T^2 \rangle] + \frac{2\langle B^2 \rangle - 3\langle B_T^2 \rangle}{r} \quad (22)$$

The above expression for the angle-averaged radial Lorentz force can be simplified for different magnetic field configurations some of which we enumerate below:

- (i) $\langle B_\theta^2 \rangle = \langle B_\phi^2 \rangle \simeq 0$ (nearly radial field):

In this case, $\langle B^2 \rangle \simeq \langle B_r^2 \rangle$. Hence

$$\langle F_r \rangle = -\frac{d}{dr} \left\langle \frac{B^2}{8\pi} \right\rangle - \frac{4}{r} \left\langle \frac{B^2}{8\pi} \right\rangle \quad (23)$$

- (ii) $\langle B_r^2 \rangle = \langle B_\theta^2 \rangle = \langle B_\phi^2 \rangle = \frac{1}{3} \langle B^2 \rangle$:

In this case, the simplified expression is,

$$\langle F_r \rangle = -\frac{1}{3} \frac{d}{dr} \left\langle \frac{B^2}{8\pi} \right\rangle \quad (24)$$

- (iii) $\langle B_\phi^2 \rangle = 0$ (poloidal field):

In this case, the simplified expression is,

$$\langle F_r \rangle = \frac{1}{8\pi} \frac{d}{dr} [B_r^2 - B_\theta^2] + \frac{2B_r^2 - B_\theta^2}{4\pi r} \quad (25)$$

For the special case of a dipole magnetic field, which we assume for calculations in this paper, we have

$$\begin{aligned} \langle B_r^2 \rangle &= \frac{B_0^2}{r^6} \int \frac{d\Omega}{4\pi} \sin^2 \theta = \frac{2B_0^2}{3r^6} \\ \langle B_\theta^2 \rangle &= \frac{4B_0^2}{r^6} \int \frac{d\Omega}{4\pi} \cos^2 \theta = \frac{4B_0^2}{3r^6} \end{aligned}$$

The Lorentz force thus can be expressed as :

$$\langle F_r \rangle = \frac{B_0^2}{12\pi r^7}$$

- (iv) $\langle B_r^2 \rangle = \langle B_\theta^2 \rangle = 0$ (toroidal field) :

In this case, the expression simplifies to:

$$\langle F_r \rangle = -\frac{d}{dr} \left\langle \frac{B_\phi^2}{8\pi} \right\rangle - \frac{B_\phi^2}{4\pi r} \quad (26)$$

For the special case of dipole field, we get

$$\langle F_r \rangle = \frac{B_0^2}{2\pi r^7}$$

5.2. Acknowledgments

R.M. thanks Grant No. SR/S2HEP12/2007, funded by DST, India for financial support. S.K.G. and S.R. thank Department of Science & Technology, Govt. of India for support under the IRHPA scheme.

References

- [1] Witten E 1984 Phys. Rev. D **30** 272
- [2] Haensel P, Zdunik J L & Schaeffer R 1986 Astronomy & Astrophysics **160** 121
- [3] Farhi E and Jaffe R L 1989 Phys. Rev. D **30** 2379
- [4] Cheng K S, Dai Z G, Wai D M & Lu T 1998 Science **280** 407
- [5] Li X D, Bombaci I, Dey M, Dey J & van der Heuvel E P J 1999 Phys. Rev. Lett. **83** 3776
- [6] Dey M, Bombaci I, Dey J & Samanta B C 1998 Phys. Lett. B **438** 123
- [7] Alcock C, Farhi E & Olinto A 1986 Astrophys. J. **310** 261
- [8] Glendenning N 1991 Nucl. Phys. (Proc. Suppl.) B **24** 110 ; 1992 Phys. Rev. D **46** 1274
- [9] Olinto A 1987 Phys. Lett. B **192** 71 ; 1991 Nucl. Phys. Proc. Suppl. B **24** 103
- [10] Madsen J & Olsen M L 1991 Nucl. Phys. (Proc. Suppl.) B **24** 170
- [11] Byam G, Heiselberg H & Pethick C J 1991 Nucl. Phys. (Proc. Suppl.) B **24** 144
- [12] Collins J & Perry M 1975 Phys. Rev. Lett. **34** 1353
- [13] Benvenuto O G & Horvath J E 1988 Phys. Lett. B **213** 516
- [14] Cho H T, Ng K W & Speliotopoulos A W 1994 Phys. Lett. B **326** 111
- [15] Tokareva I, Nusser A, Gurovich V & Folomeev V 2005 Int. J. Mod. Phys. D **14** 33
- [16] Berezhiani Z, Bombaci I, Drago A, Frontera F & Lavagno A 2003 Astrophys. J. **586** 1250
- [17] Bombaci I, Parenti I & Vidana I 2004 Astrophys. J. **614** 314
- [18] Drago A, Lavagno A & Pagliara G 2004 Phys. Rev. D **69** 057505
- [19] Alam J, Raha S & Sinha B 1996 Phys. Rep. **273** 243
- [20] Bombaci I, Logoteta D, Providencia C and Vidana I 2010 Prog. Theor. Phys. Suppl. **186** 32
- [21] Mintz B W, Fraga E S, Pagliara G and Schaffner-Bielich J 2010 Phys. Rev. D **81** 123012
- [22] Niebergal B, Ouyed R and Jaikumar P 2010 Phys. Rev. C **82** 062801
- [23] Herzog M and Ropke F K 2011 Phys. Rev. D **84** 083002
- [24] Bhattacharyya A, Ghosh S K, Joarder P, Mallick R & Raha S 2006 Phys. Rev. C **74** 065804
- [25] Bhattacharyya A, Ghosh S K, Mallick R & Raha S 2007 Phys. Rev. C **76** 052801
- [26] Michel F C 1982 Rev. Mod. Phys. **54** 1
- [27] Mallick R, Ghosh S K & Raha S 2009 arxiv:0904:3393[astro-ph.HE]
- [28] Ellis J, Kapusta J I & Olive K A 1991 Nucl. Phys. B **348** 345
- [29] Demorest P, Pennucci T, Ransom S, Roberts M & Hessels J 2010 Nature **467** 1081
- [30] Lattimer J M & Prakash M 2005 Phys. Rev. Lett. **94** 111101.
- [31] Zdunik J L, Bulik T, Kluzniak W, Haensel P & Gondek-Rosinska D 2000 Astronomy & Astrophysics **359** 143
- [32] Bauswein A, Oechslin R & Janka H T 2010 Phys. Rev. D **81** 024012
- [33] Weissenborn S, Sagert I, Pagliara G, Hempel M & Schaffner-Bielich J 2011 Astrophys. J. **740** L14.
- [34] Kurkela A, Romatschke P & Vuorinen A 2010 Phys. Rev. D **81** 105021.
- [35] Ghosh S K, Mukherjee T K, Mustafa M G & Ray R 2006 Phys. Rev. D **73** 114007.
- [36] Landau L D & Lifshitz E M 1987 *Fluid Mechanics* (Pergamon Press)
- [37] Gleeson A M & Raha S 1982 Phys. Rev. C **26** 1521
- [38] Tolman R C 1939 Phys. Rev. **55** 364
- [39] Oppenheimer J R & Volkoff G M 1939 Phys. Rev. **55** 374.
- [40] Lai D & Shapiro S L 1991 Astrophys. J. **383**
- [41] Arnett W D & Bowers R L 1977 Astrophys. J. Supp. **33** 415
- [42] Bethe H A & Johnson M 1974 Nucl. Phys. A **230** 1

- [43] Thompson C & Duncan R C 1993 *Astrophys. J.* **408** 194
- [44] Wheeler J C, Meier D L & Wilson J R 2002 *Astrophys. J.* **568** 807
- [45] Rasio F A & Shapiro S L 1992 *Astrophys. J.* **401** 226
- [46] Shibata M & Uryu K 2000 *Phys. Rev. D* **61** 064001
- [47] Lugones G, Ghezzi C R, de Gouvêa Dal Pino E M & Horvath J E 2002 *Astrophys. J. Lett.* **581** L101
- [48] Gopal R & Roychowdhury S 2010 *JCAP* **611**